

A decomposition scheme for 3D fuzzy objects based on fuzzy distance information

Stina Svensson *

Centre for Image Analysis, Swedish University of Agricultural Sciences, Lägerhyddsvägen 3, SE-75237 Uppsala, Sweden

Received 30 June 2005; received in revised form 12 June 2006

Available online 18 September 2006

Communicated by P. Bhattacharya

Abstract

A decomposition scheme for 3D fuzzy objects is presented. The decomposition is guided by a fuzzy distance transform (FDT) of the fuzzy object and aims to decompose the fuzzy object into simpler parts. Relevant voxels, corresponding to the “centres” of the parts, are detected on the FDT and suitably grouped, using a hierarchical clustering technique, into significant seeds for the decomposition. A region growing process is then applied to the seeds. The region growing process makes use of the *reverse fuzzy distance transform*, which is introduced in this manuscript. The decomposition scheme is illustrated using real data from different applications of which one, namely the identification of the three parts of the Immunoglobulin G antibody imaged using cryo electron tomography, is described more in detail.

© 2006 Elsevier B.V. All rights reserved.

Keywords: Fuzzy shape analysis; Fuzzy (reverse) distance transform; Hierarchical clustering; Cryo electron tomography; Immunoglobulin G

1. Introduction

A frequently occurring image analysis task is to, starting from a grey-level image of fairly low resolution, identify and separate blob-like structures that are clustered. With low resolution we here refer to the fact that each blob is represented only by a small number of voxels. The applications in mind are often found in biomedical cell image analysis, where the image acquisition system used typically can generate an image with a resolution higher than 1 μm . Still each blob can consist of less than 100 voxels. One such example is microscopy images of localised fluorescence signals from molecular identification events in situ (Larsson et al., 2004; Landegren et al., 2004). Separation of clustered signals, or blobs, is essential for exact positioning and counting of the number of blobs in a sample. Another

example is to identify parts of individual proteins imaged using cryo electron tomography (Bongini et al., 2004; Sintorn and Mata, 2004). The number of parts and their relative position is often the key to understanding how flexible a protein is and how it can interact with, or bind to, other proteins or substances. In both cases, no distinct borders to the background exist for the blobs of interest (fluorescence signals and parts of proteins, respectively). This, together with the fact that each blob consists only of a small number of voxels (less than 100 and less than 1500 voxels, respectively), make shape analysis difficult.

Various types of blob separation algorithms, applicable to 2D or 3D images, based on shape information can be found in the literature (Vincent, 1993; Roysam et al., 1994). In most cases, the algorithms have as an input a crisp set. Hence, a preprocessing step during which the objects of interest are delineated is necessary. For this step, a key issue is often uneven background intensity. Several approaches have been taken to treat this problem such as using flexible Poisson image models (Roysam et al., 1994)

* Tel.: +46 18 4713465; fax: +46 18 553447.

E-mail address: stina@cb.uu.se

URL: <http://www.cb.uu.se/~stina/>

or seeded watershed segmentation (Wählby et al., 2004). Once the objects of interest have been delineated they are (further) decomposed by applying shape-based segmentation method, e.g., watershed segmentation of the distance transform of the objects to be decomposed (Vincent and Soille, 1991; Vincent, 1993).

Our aim is to achieve a more robust separation by combining shape and grey-level information. We propose a decomposition scheme which can be applied to a fuzzy object, see Zadeh (1965), and uses a fuzzy distance transform, see Saha et al. (2002), as well as statistical methods for clustering of relevant voxels, see e.g., Duda et al. (2001). In this way, the preprocessing step to delineate the objects of interest is eliminated, or made less crucial for the result of the decomposition scheme. The intention with this manuscript is to present the general idea of a decomposition scheme that we believe will come useful in a number of applications, with suitable adjustments. We describe in detail the various steps of the method and illustrate its usefulness in various applications.

In Svensson and Sanniti di Baja (2002), a decomposition scheme for 3D discrete objects was presented. The decomposition scheme for 3D fuzzy objects proposed in this manuscript follows to some extent the same steps as Svensson and Sanniti di Baja (2002), but using a fuzzy setting. The decomposition scheme for 3D discrete objects uses a region growing process based on the reverse distance transform. Following the same approach, we here introduce and use the *reverse fuzzy distance transform* (RFDT). To our knowledge, the RFDT has not been used before.

The algorithm is developed for 3D fuzzy objects, as the application we have in mind is for 3D images (cryo electron tomographic images of proteins), but can equally well be applied to 2D fuzzy objects. In fact, we give examples from two different applications, one making use of 2D images (fluorescence microscopic images of tissue slices from carcinoma of the prostate) and one of 3D images. The different steps of the algorithm is illustrated on 2D images for visualization purposes. The performance on cryo electron tomographic images of proteins is described in detail in Section 5.

2. Preliminaries

We recall the definition in (Zadeh, 1965): let X be the reference set, then a *fuzzy subset* \mathcal{A} of X is defined as a set of ordered pairs $\mathcal{A} = \{(x, \mu_{\mathcal{A}}(x)) | x \in X\}$, where $\mu_{\mathcal{A}} : X \rightarrow [0, 1]$ is the *membership function* of \mathcal{A} in X . A *3D fuzzy digital object* \mathcal{O} is a fuzzy subset defined on \mathbf{Z}^3 , i.e., $\mathcal{O} = \{(p, \mu_{\mathcal{O}}(p)) | p \in \mathbf{Z}^3\}$, where $\mu_{\mathcal{O}} : \mathbf{Z}^3 \rightarrow [0, 1]$.

The notion of grey-weighted distance was introduced by Rutovitz (1968). This concept was put into a theoretical framework and denoted the fuzzy distance transform (FDT) by Saha et al. (2002). The notion of fuzzy distance between two voxels p and q is defined as being the shortest length of a path between p and q . The length $\Pi_{\mathcal{O}}(\pi)$ of a path $\pi = \langle p = p_1, \dots, p_m = q \rangle$ is

$$\Pi_{\mathcal{O}}(\pi) = \sum_{i=1}^{m-1} \frac{1}{2} (\mu_{\mathcal{O}}(p_i) + \mu_{\mathcal{O}}(p_{i+1})) \cdot \|p_i - p_{i+1}\|, \quad (1)$$

where $\|\cdot\|$ denotes the Euclidean norm and is used to calculate the local spatial distance between p_i and p_{i+1} .

As pointed out by Saha et al. (2002), the FDT can be computed using a raster scan approach similar to the one used for computing the distance transform of a 3D binary image (Borgefors, 1996). However, it is computationally inefficient due to the fact that, differently from for binary images, repeated sets of forward and backward scans are necessary. The number of iteration is different depending on the problem domain and may be large. Therefore, Saha et al. (2002) propose a dynamic programming approach for a fast implementation.

For visualization purposes (see Section 5), we in this manuscript use information from the membership function often referred to as *fuzzy connectedness*, $c_{\mathcal{A}}$ (Rosenfeld, 1979). For $c_{\mathcal{A}}$, the strength of membership of a contiguous path π_{uv} between two voxels u and v in a fuzzy subset \mathcal{A} is defined as the smallest membership value along the path and the degree of connectedness $c_{\mathcal{A}}(u, v)$ as the strongest path between u and v , i.e.,

$$c_{\mathcal{A}}(u, v) = \max_{p \in \pi_{uv}} \left[\min_{e \in \mathcal{E}(p)} \mu_{\mathcal{A}}(e) \right], \quad (2)$$

where π_{uv} is the set of all paths between u and v and $\mathcal{E}(p)$ is the set of all voxels along the path p .

Given a set of points in a feature space, in our case applied for points in \mathbf{Z}^3 , hierarchical clustering can be used to find natural clusters of the points, see, e.g., Duda et al. (2001). Hierarchical clustering is an unsupervised clustering technique, which is suitable in cases where the number of clusters is unknown. Starting from a set of p points, the first partitioning is into p clusters, the next into $p - 1$ clusters, and so on until the p th partitioning where one cluster is reached. At each level, the two clusters that are currently most similar, according to some similarity measure, are merged. The most common representation of hierarchical clustering is a corresponding tree, called *dendrogram*, showing how the points are clustered and at what degree of similarity clusters are merged. The similarity measure between two clusters is dependent on the definition of the distance between two points as well as the definition of the linking rule used for the clusters. The distance between points can be, for example, the Euclidean distance. For linkage rules, one commonly used is

$$d_{\max}(\mathcal{D}_i, \mathcal{D}_j) = \max_{x \in \mathcal{D}_i, x' \in \mathcal{D}_j} \|x - x'\|, \quad (3)$$

where \mathcal{D}_i and \mathcal{D}_j are cluster i and j . When Eq. (3) is used, the result is a so called farthest-neighbour clustering algorithm, or maximum algorithm. If the algorithm is set to terminate when the distance exceeds an arbitrary threshold, it is called *complete linkage algorithm*. This process discourages the growth of elongated clusters and is preferable to use when the true clusters are compact and roughly the same in size.

Another type of linkage is the weighted pair-group method using centroids (WPGMC) which is available in most packages for statistical analysis of data, there often referred to as median distance. It was first proposed by Gower (1967). The centroid $\bar{\mathcal{D}}_i$ for cluster i is calculated as

$$\bar{\mathcal{D}}_i = \frac{1}{n} \sum_{j=1}^n \mathbf{x}_j, \quad (4)$$

where \mathbf{x}_j are the points belonging to cluster i . The weighted centroid $\tilde{\mathcal{D}}_i$ for cluster i is defined recursively. If the cluster i is created by combining clusters p and q , then

$$\tilde{\mathcal{D}}_i = \frac{1}{2} (\tilde{\mathcal{D}}_p + \tilde{\mathcal{D}}_q). \quad (5)$$

Centroid clustering in general is based on the simple geometric assumption that the centroid of the cluster can be imaged as the type-object of the cluster. Using only the distance between centroids may introduce a bias if certain centroids are overrepresented in the data. This effect is reduced by using the described weighted approach.

A decision on the number of cluster most natural for the set is based on information of dissimilarity found in the dendrogram. For more details on hierarchical clustering, we refer to Duda et al. (2001) or any other book on statistics.

3. The reverse fuzzy distance transform

In this section, we introduce the reverse fuzzy distance transform (RFDT) as well as give implementation aspects of the FDT and the RFDT.

A (crisp) object $\mathcal{O} \in \mathbf{Z}^n$ can be treated as a set of balls $\mathcal{B}_i = \{\mathbf{x} \in \mathbf{Z}^n | d(\mathbf{c}_i, \mathbf{x}) \leq r_i\}$ for some distance function $d: \mathbf{Z}^n \rightarrow \mathbf{R}$ with centre points $\mathbf{c}_i \in \mathbf{Z}^n$ and radii $r_i \in \mathbf{R}$, for $i = 1, \dots, m$, where the union of the set, $\bigcup_{i=1}^m \mathcal{B}_i$, is equal to \mathcal{O} . Hence, \mathcal{O} can be represented by $\mathcal{S} = \{(\mathbf{c}_i, r_i) | i = 1, \dots, m\}$. \mathcal{O} is recovered from \mathcal{S} by adding a ball of radius r_i to each \mathbf{c}_i . This recovery process is efficiently implemented using the reverse distance transform (RDT). The RDT is computed by propagating local distance information in two scans over the image starting from a set of points each assigned with a distance label, e.g., \mathcal{S} , and results in an grey-level image containing a ball centred on each of the points having radius equal to the distance label of the points. See, e.g., the work by Nyström and Borgefors (1995). We remark that for a crisp object $\mathcal{O} \in \mathbf{Z}^n$, one often used \mathcal{S} is the set of centres of maximal balls from which it is guaranteed that \mathcal{O} can be recovered by the process explained above (Arcelli and Sanniti di Baja, 1988).

The RDT can be used as a region growing process, where we start from a set of seeds each assigned with a distance label as well as an identity label according to some labeling processing. The identity of each seed is propagated together with decreasing distance information. The result is that points in the image are labelled with the identity of the closest point in \mathcal{S} .

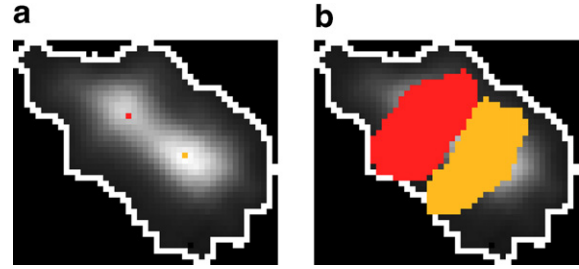


Fig. 1. (a) Fuzzy object \mathcal{O} with $\mathcal{S} = \{(c_1, r_1), (c_2, r_2)\}$ shown overlaid. (b) Fuzzy balls grown from \mathcal{S} .

We generalize RDT to a fuzzy setting resulting in the reverse fuzzy distance transform (RFDT). In this case, decreasing fuzzy distances are propagated on the fuzzy object. We illustrate the effect using a synthetic image example. In Fig. 1(a), a 2D fuzzy object \mathcal{O} is shown. Its support is outlined for easier interpretation. The set $\mathcal{S} = \{c_1, c_2\}$ is shown overlaid. r_i is set to be equal to the shortest fuzzy distance from c_i to the complement of the support of \mathcal{O} . The fuzzy balls corresponding to \mathcal{S} are shown in Fig. 1(b). Due to the choice of r_i , the fuzzy balls will reach the border of \mathcal{O} , but not further. In places where a pixel can be reached both from c_1 and from c_2 , the identity is set to be the one giving the shortest fuzzy distance to the seed. The fuzzy balls are diagonally elongated due to the distribution of the membership values in \mathcal{O} .

Saha et al. (2002) suggested to use the Euclidean distance as the spatial local distance between voxels when computing the FDT (Eq. (1)). We use Eq. (1) for the computation of the FDT and the RFDT but with the $\langle 3, 4, 5 \rangle$ distance, i.e., the local spatial distance between two face neighbours is weighted 3, two edge neighbours 4, and two vertex neighbours 5, instead of the Euclidean distance following the concept of weighted distance transforms for binary images (Borgefors, 1996). By using the $\langle 3, 4, 5 \rangle$ distance, we can work with integer numbers and still achieve a good approximation of the Euclidean distance.

As mentioned in Section 2, Saha et al. (2002) suggest to use dynamic programming for an efficient implementation of the FDT. For simplicity we use repeated raster scans. Increasing distances are propagated over the image in repeated sets of forward and backward scans. The FDT is found as soon as no further updating of distance labels are done during one complete set of scans. The algorithm is similar to that of computing a distance transform of a binary image (Borgefors, 1996), with the difference that for a binary image only one set of scans is necessary. When the $\langle 3, 4, 5 \rangle$ distance is used for calculating the FDT, information from a $3 \times 3 \times 3$ neighbourhood of the voxel v , i.e., its 26 nearest neighbours, is taken into account. For a voxel v , its already visited neighbours (during the current scan), n_1, \dots, n_{13} , are investigated. For each n_m , the fuzzy distance from the border of \mathcal{O} to v passing through n_m is computed. This is done by adding the local fuzzy distance between v and n_m to the fuzzy distance value currently stored in n_m . If any shorter path is found than the one

already stored in v , the fuzzy distance value of v is updated with the found smaller value. The local fuzzy distance between v and n_m is given by Eq. (1).

The algorithm for computing the FDT is formalized by the following. The weights used in the forward and the backward scans for estimating the local spatial distance between v and n_m based on the $\langle 3, 4, 5 \rangle$ distance are found in Fig. 2. The weights are denoted by $w(i, j, k)$, where $i = -1, 0, 1$; $j = -1, 0, 1$; and $k = -1, 0, 1$ correspond to the local x -, y -, z -coordinates of the voxels n_m , $m = 1, \dots, 26$, around v . The local coordinates (i, j, k) used in the forward scan are said to belong to the set F and the one used in the backward scan to the set B . One set of forward and backward scans for the computation of the FDT of an image I of size $X \times Y \times Z$ can then be summarized by the following pseudo code. Note that for voxels placed on the image border, the weight mask is suitably reduced.

for $z = 1$ to Z

 for $y = 1$ to Y

 for $x = 1$ to X

$$I(x, y, z) = \min_{(i, j, k) \in F} \left[I(x + i, y + j, z + k) + \frac{1}{2}(\mu_{\mathcal{O}}(x, y, z) + \mu_{\mathcal{O}}(x + i, y + j, z + k)) \cdot w(i, j, k) \right]$$

for $z = Z$ downto 1

 for $y = Y$ downto 1

 for $x = X$ downto 1

$$I(x, y, z) = \min_{(i, j, k) \in B} \left[I(x + i, y + j, z + k) + \frac{1}{2}(\mu_{\mathcal{O}}(x, y, z) + \mu_{\mathcal{O}}(x + i, y + j, z + k)) \cdot w(i, j, k) \right]$$

The RFDT can be computed using repeated raster scans in a similar way as is described above for the FDT with the difference that decreasing instead of increasing distances

are propagated from the input voxels. The RFDT is found as soon as no further updating of distance labels are done during one complete set of scans. For a voxel v , its already visited neighbours (during the current scan), n_1, \dots, n_{13} , are investigated. For each n_m , the fuzzy distance information propagated from the input voxels to v passing through n_m is computed. This is done by *subtracting* the local fuzzy distance between v and n_m from the fuzzy distance value currently stored in n_m . If any larger fuzzy distance value is found than the one already stored in v , the fuzzy distance value of v is updated with the found larger value. The local fuzzy distance between v and n_m is again given by Eq. (1). Note that for the computation of the local fuzzy distance, $\mu_{\mathcal{O}}(v)$ and $\mu_{\mathcal{O}}(n_m)$ need to be known. This means that the RFDT is actually computed on the fuzzy object \mathcal{O} . The algorithm for computing the RFDT is formalized in the same way as for the FDT, again with the difference that the local fuzzy distance is subtracted instead of added.

4. A decomposition scheme for fuzzy objects

In this section, the decomposition scheme for fuzzy objects is described and motivated.

Our aim is to identify individual blob-like structures from a cluster consisting of blob-like structures represented as a fuzzy object. A small example of such a situation is shown in Fig. 3. It corresponds to part of an optical slice from a 3D image of fluorescence labeled detection probes aimed for mitochondrial DNA in vitro (Larsson et al., 2004). As mentioned in the Introduction, typical for the objects we have in mind is that the resolution is poor, in the sense that each blob consists of a rather small number of voxels (e.g., the blobs in Fig. 3 are less than 50 pixels each). Moreover, no distinct borders exist, hence making it difficult to delineate the object from the background. These two facts make binary shape analysis difficult and (presumably) with unstable results. We therefore propose a fuzzy setting.

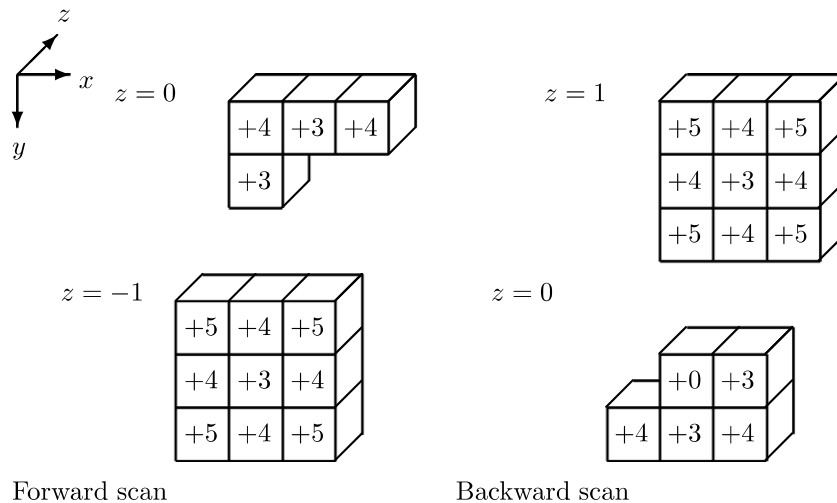


Fig. 2. Weights for the estimating the local spatial distance between two voxels used in Eq. (1).

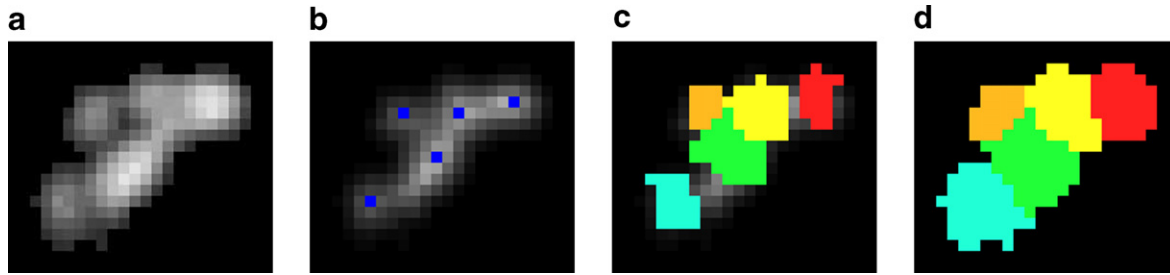


Fig. 3. Decomposition of a cluster of blob-like structures: (a) the membership values; (b) local maxima shown overlaid on the FDT; (c) fuzzy balls grown from the seeds; (d) decomposition of the fuzzy object.

For binary objects, the most internal part of a convex blob is identified as being one or several local maxima of the distance transform (DT), see, e.g., Svensson and Sanniti di Baja (2002). However, an initial binarisation process is necessary. Instead, we compute the FDT of the fuzzy object corresponding to the blob-like structure of interest. In the same way as for the DT of a binary object, locally maximal fuzzy distance values are found in correspondence with the most internal parts of fuzzy blobs. Local maxima of the FDT are identified and used as seeds for the decomposition scheme.

In Fig. 3(b), the FDT of the fuzzy object in Fig. 3(a) is shown with its five local maxima overlaid.

In the ideal case, we have one local maximum corresponding to each blob in the cluster, as for the example in Fig. 3. However, this is not always the case when working with real data. The fuzzy border can be jagged as in Fig. 4, where a synthetic fuzzy object is shown. In this example, four local maxima are found corresponding to two blobs. To reduce this effect, smoothing can be applied as a preprocessing step. We use a different approach to have more control over the process. Local maxima corresponding to the same blob are presumably spatially close and are therefore grouped using a clustering technique. For this purpose, local maxima are labelled (using the algorithm described in Thurffjell et al. (1992)) and hierarchical clustering is applied. The reason for choosing hierarchical clustering is that the number of groups is in most cases not known a priori. In such cases, an analysis of the resulting dendrogram is used to take a decision on the number of groups most suitable for the processed data set according

to some application dependent criteria. Such criterion could be, for example, largest accepted diameter of a cluster set, which would correspond to a threshold on the smallest expected distance between blobs (Duda et al., 2001).

In the following, we denote each resulting cluster a *seed*. Hence, a seed consists of a number of voxels having the same identity label. Each voxel in the seed has, together with an identity label, a fuzzy membership value as well as a fuzzy distance value. The fuzzy membership values and the fuzzy distance values are used in the region growing process that follows.

Once the seeds are identified, a region growing process is applied to the seeds. In order to have a fuzzy shape based region growing process, we use the RFDT. The RFDT is computed starting from the seeds. Decreasing fuzzy distance information is propagated together with the identity label of the seed. In this way, a fuzzy ball of radius equal to the FDT value of the voxel is grown from each local maximum and each voxel is assigned the identity label of its closest seed, according to the fuzzy distance. The membership values needed to compute the RFDT are found on the fuzzy object for which the FDT was computed. The RFDT is computed once, treating all seeds simultaneously. Due to the properties of the RFDT, the union of the fuzzy balls is a subset of the original fuzzy object.

In general, the fuzzy balls are not enough to assign all voxels in the fuzzy object with an identity label. This is due to the fact we calculate fuzzy balls starting from the set of local maxima found on the FDT and not from the set of *centres of maximal fuzzy balls*, the analogy of centres

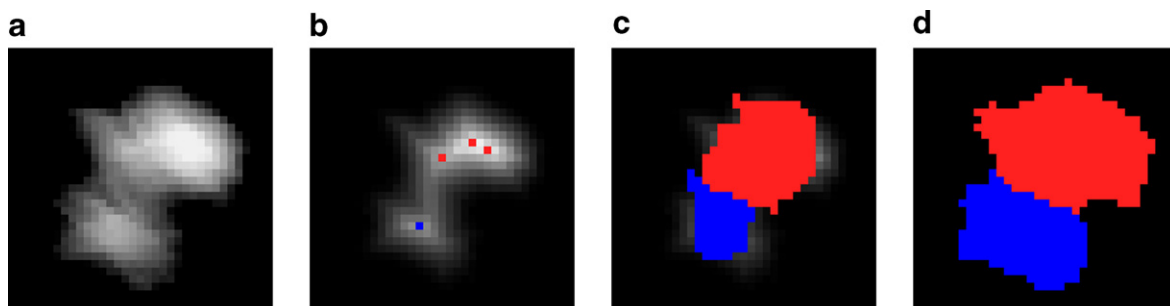


Fig. 4. Decomposition of a synthetic fuzzy object: (a) membership values; (b) seeds (consisting of two groups of local maxima) shown overlaid on the FDT; (c) fuzzy balls grown from the seeds; (d) decomposition of the fuzzy object.

of maximal balls for the crisp case. To our knowledge, this latter concept is still left to be defined and is a research topic of its own. In this manuscript, we limit ourselves to using local maxima and therefore, a second step of region growing is necessary. Non-labelled voxels are ascribed to their closest part, according to the fuzzy distance. For this purpose, we compute the FDT starting from the already identified parts. Fuzzy distance information is propagated together with the identity label. In the same way as for the RFDT, the FDT is only computed once, treating all parts simultaneously.

The results after applying the RFDT are shown in Figs. 3(c) and 4(c) and the final decompositions in Figs. 3(d) and 4(d), respectively.

Most voxels are assigned during the first step of region growing (102 out of 186 for the example in Fig. 3 and 291 out of 455 for the example in Fig. 4).

To summarize, the decomposition scheme consists of the following steps:

- (1) computing the FDT of the fuzzy object to be decomposed,
- (2) identifying local maxima on the FDT,
- (3) grouping of local maxima into seeds by hierarchical clustering,
- (4) region growing to identify the parts corresponding to the seeds
 - (a) growing of fuzzy balls for the seeds by computation of the RFDT, including propagation of seed identity,
 - (b) ascribing identity to the remaining voxels in the fuzzy object by computation of the FDT, including propagation of seed identity.

The computational complexity to a large extent depends on the number of scans necessary to compute the FDT and the RFDT, respectively. This number differs depending on the image content. Typical for the images shown in this manuscript is that two to three sets of forward and backward scans are needed each time the FDT or the RFDT is computed. Each scan is fast as it only involves local computations around each pixel.

The usefulness of (3), grouping of local maxima into seeds by hierarchical clustering, is illustrated on the image shown in Fig. 5(a), a fluorescence microscopic image of a 10 μm tissue slice from carcinoma of the prostate. Cell nuclei are stained with the fluorescent dye DAPI and the pixel-size is $0.1 \times 0.1 \mu\text{m}$. The image belongs to a set of images used in a study by Erlandsson et al. (2003). The fuzzy objects are identified using one of the fuzzy segmentation methods presented by Pal and Rosenfeld (1988) (minimization of fuzziness using entropy as a measure of fuzziness) and are shown in Fig. 5(b). Following the proposed decomposition scheme, the FDT is computed and local maxima are identified. The local maxima are grouped into seeds using hierarchical clustering with Euclidean distance and WPGMC linkage. We use WPGMC as it is likely that the local maxima of each cell nuclei is located near its centroid. As mentioned in Section 2, the weighting used in WPGMC is intended to reduce the bias that may occur if certain centroids are overrepresented in the data. The choice of WPGMC, instead of a similar non weighted centroid based linkage, is reasonable as we may have many local maxima. Clusters are formed as long as the Euclidean distance between the clusters is less than 25 pixels, an assumption based on a priori knowledge of the image data. In Fig. 5(c), the seeds resulting after grouping of local maxima are shown overlayed on the FDT. In Fig. 5(d), the final decomposition is shown. As can be seen in the image, cell nuclei are identified in a satisfactory way except in a few cases where the nuclei are partially outside the image.

The above proposed decomposition scheme differs from the method proposed by Svensson and Sanniti di Baja (2002) essentially in two ways. There, a segmentation of the image into object and background is required. Furthermore, there is no clustering technique involved to group the local maxima. Instead, a suitable subset of the set of centres of maximal balls is used and the voxels in this set are grouped into seeds by merging spatially close voxels using morphological operations. Bengtsson et al. (2004) propose a cell segmentation algorithm based on watershed segmentation of the FDT computed from a fuzzy thresholded image obtained by the same method as is used for Fig. 5. The method is described for 2D images, but is easy to

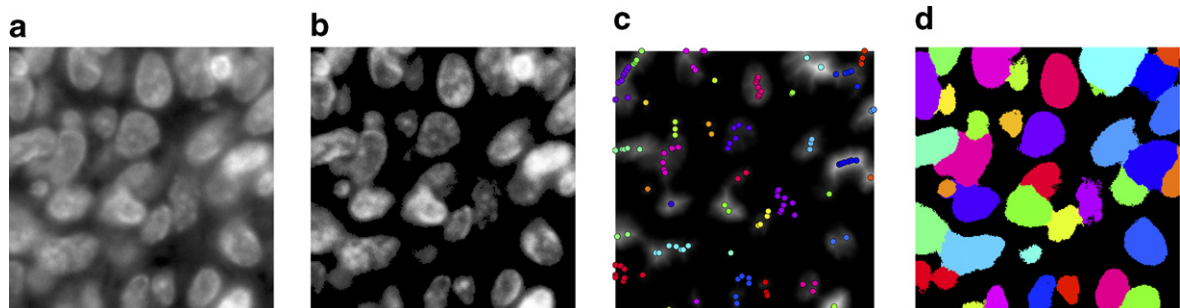


Fig. 5. Decomposition of a fluorescence microscopic image of a tissue slice from carcinoma of the prostate: (a) original image; (b) fuzzy objects; (c) seeds shown overlayed on the FDT; (d) resulting decomposition.

generalize to 3D images. Also compared with Bengtsson et al. (2004), there are essentially two differences with our method. No clustering is used for grouping of local maxima. Instead the local maxima are reduced by the h -extrema transformation (Soille, 1999), which suppresses all maxima whose depth is smaller than a threshold h . Despite suppression of shallow local maxima, the method results in an oversegmentation of the objects and, hence, the need of a subsequent merging process. Moreover, region growing is performed by using watershed segmentation applied to the FDT instead of the here proposed use of the RFDT. By using hierarchical clustering of local maxima as is proposed in this manuscript, a priori knowledge of the imaged material, such as shape, is easier to incorporate in the algorithm. This together with the fact that no segmentation of the image into object and background, which is necessary for the method proposed in (Svensson and Sanniti di Baja, 2002), are the advantages of our method.

5. Application of the decomposition scheme to cryo electron tomographic data of proteins

The motivation for this work originates from a cooperation with the Department of Cell and Molecular Biology, Karolinska Institute, Stockholm, Sweden. Proteins, for example the Immunoglobulin G (IgG) antibody, are imaged individually using cryo electron tomography (cryo-ET) and analyzed with respect to protein dynamics to study the flexibilities of the antibody (Bongini et al., 2004). The step from image acquisition to a suitable model for the dynamic system has so far been done manually. For large-scale studies, an automatic procedure is required. The first step in such an automatic procedure is to identify the different parts each protein consists of, i.e., the effector domain (Fc stem) and its two fragment antigen-binding arms (Fab arms) for the IgG antibody. See Fig. 6(a), where three examples of IgG antibodies are shown. The Fc stem is the lowest part in each of the shown antibodies. The size of an IgG antibody in a cryo-ET image is around 1500 voxels

with the used sampling (Creighton, 1993), pixel size 5.24 Å and resolution 20 Å. For such a small object, shape analysis applied to binarised data usually turns out to be non-robust. For a detailed description on the cryo-ET experiments, we refer to Sandin et al. (2004); Bongini et al. (2004).

The grey-level for a voxel in a cryo-ET image reflects the density of the imaged object in that specific point. Hence, for this application, the fuzzy membership value for a voxel is set to be proportional to its grey-level.

We apply the decomposition scheme for fuzzy objects described in Section 4. For the hierarchical clustering, we use Euclidean distance and complete linkage. In this case, we use the a priori knowledge that the fuzzy object should be decomposed into three parts. This means that the local maxima will be grouped into three seeds that are spatially as distant as possible. We remark that when the number of clusters are known a priori, k -means clustering could be used for grouping of local maxima. However, we prefer to follow the general framework of the proposed decomposition scheme for fuzzy objects. Complete linkage is chosen to discourage the growth of elongated clusters (Duda et al., 2001).

The decomposed IgG antibodies are shown in Fig. 6(b).

As explained above, the decomposition scheme is applied directly to the grey-level image. For visualization purposes, we compute the fuzzy connectedness c_{α} (see Eq. (2)) from the seeds and in Fig. 6(b), visualize only voxels with fuzzy connectedness to the seed larger than a threshold α . α is chosen in such a way that the volume of the corresponding crisp set is approximately what would be expected for an IgG antibody being a 150 kDa macromolecule, i.e., 1500 voxels (Sandin et al., 2004; Creighton, 1993). The reason why we use fuzzy connectedness, instead of a simple thresholding of the original grey-level image, is the presence of noise in the images as well as the possibility of interference with adjacent objects. Neither of the two effect the decomposition scheme, but only effect the binarisation.

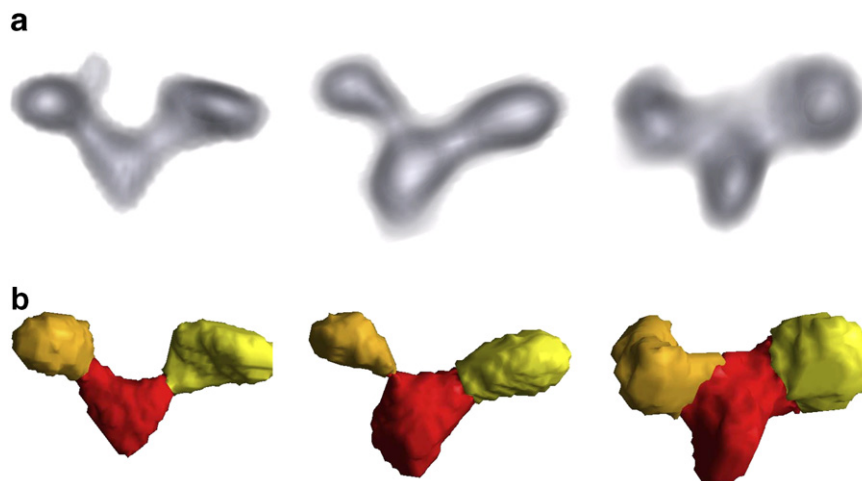


Fig. 6. (a) Volume rendering of three antibody IgG imaged by cryo-ET. (b) Surface rendering of the corresponding decomposed fuzzy objects.

The resulting decompositions (Fig. 6(b)) have been visually evaluated by experts at the Department of Cell and Molecular Biology and the identified parts correspond to the Fc stem and the two Fab arms in a satisfactory way.

In order to obtain an objective evaluation of the decomposition scheme, we have constructed noise free images from the protein's atom positions deposited in a protein data bank (PDB) (Berman et al., 2000). From a PDB entry, a volume image, where the grey-level depict density, can be generated by placing a gauss kernel at each atom position and multiply by the mass of that atom (Pittet et al., 1999). The total density, or grey-level, in a voxel is then calculated by adding the contributions from gauss kernels of atoms in the vicinity of the voxel. We have done this construction for the protein itself as well as for the Fc stem and the two Fab arms separately. Thus we have created a fuzzy object \mathcal{O} for which we know the identity of its different parts. In Fig. 7, the parts obtained from PDB data and the result when applying the decomposition scheme to \mathcal{O} are shown. \mathcal{O} consists of 2451 voxels. In the PDB data, 884 voxels belong to the Fc stem, 763 voxels to one of the Fab arms and 804 to the other Fab arm. In the decomposed object, the same parts are 888, 759, and 804 voxels respectively. In total, less than 1.0% voxels were assigned to an erroneous part.

In Sintorn and Mata (2004), an algorithm (inspired by Svensson and Sanniti di Baja (2002)) for identifying the different parts of proteins in cryo-ET images was presented. There, a delineation of the object is necessary. Thereafter, the method operates on the initial grey-level image to find local maxima. No clustering technique is used to group the local maxima. This means that the resulting decomposition may consist of more (or less) parts than what is known a priori. The decomposition scheme for fuzzy objects proposed here can be seen as an improvement of the method by Sintorn and Mata (2004).

6. Discussion

We have presented a decomposition scheme for 3D fuzzy objects. The decomposition scheme can be used in many different applications. Specifically, we have shown how it can be adapted to cryo-ET images of IgG antibodies and that it, in this case, provides a robust decomposition

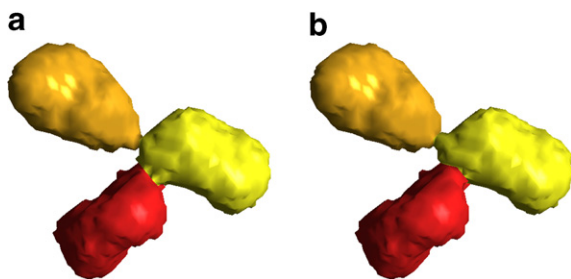


Fig. 7. Synthetic fuzzy object \mathcal{O} (PDB ID 1igt): (a) parts obtained from the PDB data and (b) the result when applying the decomposition scheme to \mathcal{O} .

into parts relevant for this specific antibody. The examples shown here are part of a larger study where 58 IgG antibodies have been studied (Svensson et al., 2006). Of these, 51 gave satisfactory results. The cases where the algorithm failed was due problems with the image acquisition resulting in too low quality images. The validation was done visually by experts at the Department of Cell and Molecular Biology.

The IgG antibodies used for this manuscript are well separated from other fuzzy objects, hence there are no problems involving adjacent fuzzy objects. More in general, the decomposition scheme for 3D fuzzy objects is intended to be used as a blob separation algorithm (see Fig. 5). In this case, the focus is to do the actual separation. A subsequent analysis is then required to identify which parts belong to which fuzzy object, if that information is of interest.

The proposed algorithm contains a number of steps which can be adjusted to suite the application at hand. Those will be discussed below, giving suggestions of suitable modifications.

In most applications, it will be necessary to start from a fuzzy object, not as for the cryo-ET images where we start directly from the grey-level image. In such cases, more sophisticated membership functions may be required to identify the fuzzy object in a proper way. The membership function may differ depending on the problem domain. See Udupa and Saha (2003) for a recent review on the concept of fuzzy connectedness and how it can be used in image segmentation.

Instead of local maxima, extended maxima (Soille, 1999) can be used to reduce the effect of noise. Extended maxima are regional maxima of the h -extrema transformation, which, in turn, is a tool to filter the image extrema using a contrast criterion, where all maxima whose depths are smaller than a threshold h are suppressed.

In the application shown in Section 5 (cryo-ET data), it was known a priori that each fuzzy object consists of three parts and, hence, should be decomposed into three parts. This means that it is possible to use k -means clustering, where $k = 3$, instead of hierarchical clustering. In other applications, another number may be used or, which is more likely, it can be the case that such a priori knowledge does not exist as for the example shown in Fig. 5. In the latter case, the dendrogram computed during the hierarchical clustering should be analyzed to find which is the suitable number of clusters for the set of local maxima at hand. Moreover, for all examples in this manuscript the Euclidean distance was used. In other applications, the fuzzy distance between the local maxima is likely to be more suitable for the hierarchical clustering. In fact, it is more probable that the local maxima are close in fuzzy distance sense than actually spatially close. This issue is currently investigated. See Gedda and Svensson (2006) for some preliminary results.

The output from this algorithm is a crisp decomposition of a fuzzy object. One step further would be to develop a

fuzzy decomposition scheme, i.e., resulting in a fuzzy decomposition of a fuzzy object (allowing overlapping parts).

Future work will be to evaluate the performance of the proposed decomposition scheme for 3D fuzzy object for other applications after suitable application dependent modifications.

Acknowledgements

Dr. Joakim Lindblad, Centre for Image Analysis, Swedish University of Agricultural Sciences, Uppsala, Sweden, is gratefully acknowledged for scientific support.

The cryo-ET data sets have been provided by Dr. Sara Sandin, Department of Cell and Molecular Biology, Karolinska Institutet, Stockholm, Sweden (currently Division of Structural Studies, MRC Laboratory of Molecular Biology, Cambridge, United Kingdom), the optical slice from a 3D image of fluorescence labeled detection probes by Sara Henriksson, Department of Genetics and Pathology, Uppsala University, Sweden, and the fluorescence microscopic image of a tissue slice from carcinoma of the prostate by Dr. Fredrik Erlandsson, Cancer Center Karolinska, CCK R8:04, Karolinska University Hospital Solna, Karolinska Institutet, Stockholm, Sweden.

Thanks also to Prof. Ulf Skoglund and Dr. Duccio Fanelli, Department of Cell and Molecular Biology, Karolinska Institutet, Stockholm, Sweden, for the evaluation of the results and to Magnus Gedda and Dr. Carolina Wählby, Centre for Image Analysis, Uppsala University, Sweden for their scientific support.

Stina Svensson is financially supported by Swedish Research Council (Project 621-2005-5540).

References

- Arcelli, C., Sanniti di Baja, G., 1988. Finding local maxima in a pseudo-Euclidean distance transform. *Comput. Vision, Graphics, Image Process.* 43 (3), 361–367.
- Bengtsson, E., Wählby, C., Lindblad, J., 2004. Robust cell image segmentation methods. *Pattern Recognition Image Anal.* 14 (2), 157–167.
- Berman, H.M., Westbrook, J., Feng, Z., Gilliland, G., Bhat, T.N., Weissig, H., Shindyalov, I.N., Bourne, P.E., 2000. The protein data bank. *Nucleic Acids Res.* 28 (1), 235–242.
- Bongini, L., Fanelli, D., Piazza, F., De Los Rios, P., Sandin, S., Skoglund, U., 2004. Freezing immunoglobulins to see them move. *Proc. Natl. Acad. Sci. (PNAS)* 101 (17), 6466–6471.
- Borgefors, G., 1996. On digital distance transforms in three dimensions. *Comput. Vision and Image Understanding* 64 (3), 368–376.
- Creighton, T.E., 1993. *Proteins: Structures and Molecular Properties*, second ed. W.H. Freeman and Company.
- Duda, R.O., Hart, P.E., Stork, D.G., 2001. *Pattern Classification*, second ed. John Wiley and Sons, Inc.
- Erlandsson, F., Wählby, C., Ekholm-Reed, S., Hellström, A.-C., Bengtsson, E., Zetterberg, A., 2003. Abnormal expression pattern of cyclin E in tumour cells. *Internat. J. Cancer* 104 (3), 369–375.
- Gedda, M., Svensson, S., 2006. Fuzzy distance based hierarchical clustering calculated using the A* algorithm. In: Reulke, R., Eckardt, U., Flach, B., Knauer, U., Polthier, K. (Eds.), *Combinatorial Image Analysis: 11th International Workshop, IWCI 2006*, Berlin, Germany, June 19–21, 2006, *Proceedings. Lecture Notes in Computer Science*, Vol. 4040. Springer Verlag, pp. 101–115.
- Gower, J.C., 1967. A comparison of some methods of cluster analysis. *Biometrics* 23 (4), 623–637.
- Landegren, U., Schallmeiner, E., Nilsson, M., Fredriksson, S., Banér, J., Gullberg, M., Jarvius, J., Gustafsdottir, S., Dahl, F., Söderberg, O., Ericsson, O., Stenberg, J., 2004. Molecular tools for a molecular medicine: analyzing genes, transcripts and proteins using padlock and proximity probes. *J. Mol. Recognition* 17, 194–197.
- Larsson, C., Koch, J., Nygren, A., Raap, A.K., Landegren, U., Nilsson, M., 2004. In situ genotyping individual DNA molecules by target-primed rolling-circle amplification of padlock probes. *Nature Methods* 1 (3), 227–232.
- Nyström, I., Borgefors, G., 1995. Synthesising objects and scenes using the reverse distance transformation in 2D and 3D. In: Braccini, C., Floriani, L.D., Vernazza, G. (Eds.), *Proc. ICIAP'95: Image Analysis and Process.* Springer-Verlag, pp. 441–446.
- Pal, S.K., Rosenfeld, A., 1988. Image enhancement and thresholding by optimization of fuzzy compactness. *Pattern Recognition Lett.* 7 (2), 77–86.
- Pittet, J.-J., Henn, C., Engel, A., Heymann, J.B., 1999. Visualizing 3D data obtained from microscopy on the internet. *J. Struct. Biol.* 125, 123–132.
- Rosenfeld, A., 1979. Fuzzy digital topology. *Inform. Control* 40 (1), 76–87.
- Roysam, B., Ancin, H., Bhattacharjya, A.K., Chisti, M.A., Seegal, R., Turner, J.N., 1994. Algorithms for automated characterization of cell populations in thick specimens from 3-D confocal fluorescence microscopy data. *J. Microscopy* 173 (2), 115–126.
- Rutovitz, D., 1968. Data structures for operations on digital images. In: Cheng, G.C., Pollock, D.K., Rosenfeld, A. (Eds.), *Pictorial Pattern Recognition*. Thompson, Washington, pp. 105–133.
- Saha, P.K., Wehrli, F.W., Gomberg, B.R., 2002. Fuzzy distance transform: Theory, algorithms, and applications. *Computer Vision and Image Understanding* 86, 171–190.
- Sandin, S., Öfverstedt, L.-G., Wikström, A.-C., Wrangé, O., Skoglund, U., 2004. Structure and flexibility of individual immunoglobulin G molecules in solution. *Structure* 12 (3), 409–415.
- Sintorn, I.-M., Mata, S., 2004. Using grey-level and shape information for decomposing proteins in 3D images. In: *IEEE International Symposium on Biomedical Imaging: Macro to Nano, 2004. (ISBI 2004)*. Vol. 1. Arlington, VA, USA, pp. 800–803.
- Soille, P., 1999. *Morphological Image Analysis*. Springer-Verlag.
- Svensson, S., Gedda, M., Fanelli, D., Skoglund, U., Öfverstedt, L.-G., Sandin, S., 2006. Using a fuzzy framework for delineation and decomposition of immunoglobulin G in cryo electron tomographic images. In: Tang, Y.Y., Wang, S.P., Lorette, G., Yeung, D.S., Yan, H. (Eds.), *Proceedings of the 18th International Conference on Pattern Recognition (ICPR 2006)*, Vol. 4. IEEE Computer Society, pp. 520–523.
- Svensson, S., Sanniti di Baja, G., 2002. Using distance transforms to decompose 3D discrete objects. *Image Vision Comput.* 20 (8), 529–540.
- Thurfjell, L., Bengtsson, E., Nordin, B., 1992. A new three-dimensional connected components labeling algorithm with simultaneous object feature extraction capability. *CVGIP: Graphical Models Image Process.* 54 (4), 357–364.
- Udupa, J.K., Saha, P.K., 2003. Fuzzy connectedness and image segmentation. *Proc. IEEE* 91 (10), 1649–1669.
- Vincent, L., 1993. Morphological grayscale reconstruction in image analysis: Applications and efficient algorithms. *IEEE Trans. Image Process.* 2 (2), 176–201.
- Vincent, L., Soille, P., 1991. Watersheds in digital spaces: An efficient algorithm based on immersion simulations. *IEEE Trans. Pattern Anal. Machine Intell.* 13 (6), 583–597.
- Wählby, C., Sintorn, I.-M., Erlandsson, F., Borgefors, G., Bengtsson, E., 2004. Combining intensity, edge, and shape information for 2D and 3D segmentation of cell nuclei in tissue sections. *J. Microscopy* 215 (1), 67–76.
- Zadeh, L.A., 1965. Fuzzy sets. *Inform. Control* 8, 338–353.